

EXHIBIT 5

Harvard Medical School

Harvard TH Chan School of Public Health

John J. Godleski, M.D.
Professor of Pathology
Emeritus



Department of
Environmental Health
(MIPS Program)

jgodlesk@hsph.harvard.edu

Phone (617) 698-5970

Cell (617) 840-9679

July 21, 2021

David Dearing, ESQ
Beasley Allen Law Firm
218 Commerce Street
Montgomery, AL 36104

Re: Anna Gallardo

Dear Mr. Dearing:

I was on the faculty of Harvard Medical School (HMS), Brigham and Women's Hospital (BWH), and Harvard School of Public Health (HSPH) from 1978-2017, retiring as Professor of Pathology in 2017. I graduated from the University of Pittsburgh School of Medicine. As a student, I did research in the Pathology Department learning electron microscopy. In my senior year, I received the top award for research done by a medical student in the United States given by the Student American Medical Association, and published several papers describing that research. I then did an internship and residency in Pathology at the Massachusetts General Hospital, a major teaching hospital of Harvard Medical School. I received further training at HSPH and the University of North Carolina. I was board certified in Anatomic Pathology in 1975. I spent 5 years on the faculty of Medical College of Pennsylvania in Philadelphia in the Department of Pathology where I was in charge of the electron microscopy facility and the autopsy service, and then was recruited to head Pulmonary Pathology at BWH in Boston, a position I held for 37 years. I published more than one hundred and seventy peer-reviewed papers related to pulmonary/environmental pathology including a number using analytical electron microscopy. Notably, I have been senior author on a number of papers using analytical electron microscopy with both X-ray analysis and electron energy loss spectroscopy. In my career, I received more than \$30 million in research grants from NIH, EPA, and other funding agencies as Principal Investigator; I led the Particles Research Core in the Harvard-NIEHS Environmental Research Center and I was Associate Director of the Harvard Clean Air Research Center supported by the US EPA. In my daily activities, I was a member of the Pulmonary Pathology and Autopsy Services at Brigham and Women's Hospital. I taught Pathology residents and fellows, medical students, graduate students, and postdoctoral fellows, and I carried out research in my laboratory at HSPH. I was responsible for accurate pathological diagnoses at BWH and I oversaw a research group of as many as 15 people at HSPH. I was the pathologist providing the final opinion on difficult diagnostic cases of lung disease within our department, and I was a recognized expert whose opinion was sought by pathologists from other hospitals in the diagnosis of foreign material in tissues throughout the body using scanning electron microscopy (SEM) and energy dispersive X-ray analyses (EDS). Although now retired, I have full access to laboratory and electron microscopy facilities.

I have recently published six papers regarding talc and tissue pathology (references 1-6). The first paper used tissue digestive procedures and SEM/EDS to quantify talc in lymph nodes in comparison to the use of *in situ* SEM/EDS; the second described the migration and detection of talc in pelvic tissues from the perineum in a series of exposed patients who also had ovarian malignancy. The third concerned the use of spectroscopic magnesium and silicon weight % ratio standards to diagnose talc in human tissues, and the expected

mathematical distribution for such measurements. Three other publications also pertain to talc identification in tissue and resultant pathology (references 4-6).

I have reviewed 66 slides on Anna Gallardo, which represent 65 histological slides (S13-28714) made from the tissues from the patient's surgical procedure on [REDACTED] which included [REDACTED]

[REDACTED]. According to the surgical pathology report, [REDACTED]. There are multiple histologic levels/ recuts for some blocks, and additionally, two frozen section slides were received (labeled FS1-1 and FS1-2) that, according to the report are derived from the same tissue in block A1. Also received was a single slide labeled M13-3243, which is a cytologic preparation ("pelvic washing") without malignant cells. Slides of S13-28714 were received with the following sublabels: A1-A8 ([REDACTED]); B1-B18 ([REDACTED]), C1, D1, E1, F1, G1, and H1 ([REDACTED]), I1-I2 ([REDACTED]), J1-J2 ([REDACTED]), K1-K2 ([REDACTED]), L1-L2 ([REDACTED]), M1-M2 ([REDACTED]), N1-N2 ([REDACTED]), O1-O5 ([REDACTED]), and P1 ([REDACTED]). All slides were prepared by the Department of Pathology at Barnes-Jewish Hospital at Washington University Medical Center, St. Louis, MO 63110. The histologic slides listed above were reviewed with light microscopy, and the diagnosis of poorly differentiated endometrioid adenocarcinoma of the ovary was confirmed. In the surgical pathology report, [REDACTED]

[REDACTED] **Figure 1** illustrates key microscopic findings of the typical areas of the patient's endometrioid carcinoma.

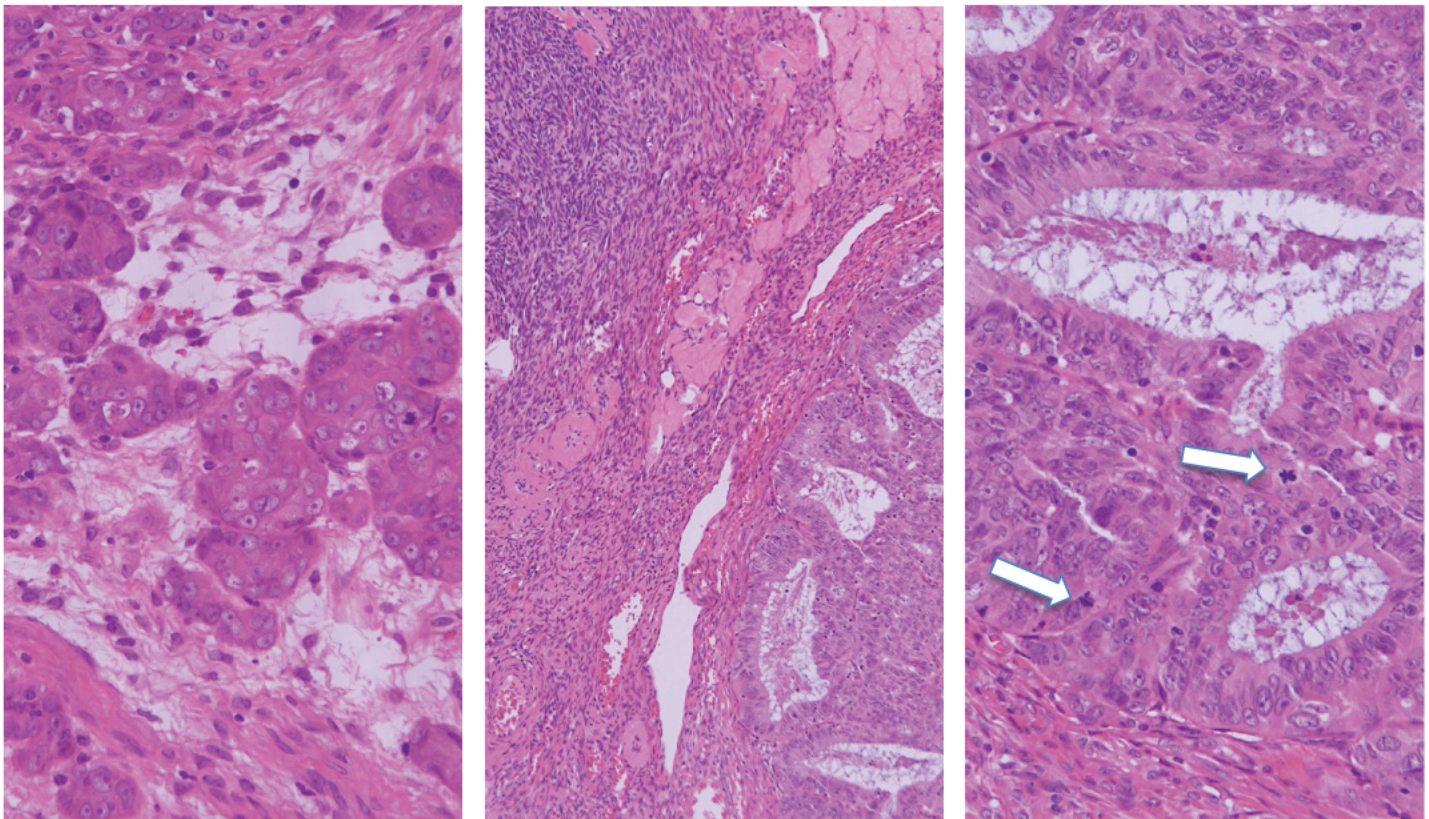


Figure 1. **Left.** High-power microscopic view of her endometrioid carcinoma of the left ovary, with large, dysplastic cells with necrosis. Original Magnification 400X. **Center.** Low power microscopic view of the tumor in the right ovary shows a distinctly glandular architecture reminiscent of endometrium. Original magnification 60x. **Right.** High-power view of her endometrioid carcinoma, showing marked nuclear pleomorphism, a generally columnar cellular architecture, and scattered mitotic figures (arrows). Original magnification 400x.

The 65 histologic slides on case S13-28714 were also reviewed using polarized light microscopy, as a means to highlight and detect birefringent foreign material in the same plane of focus with the tissues. Birefringent particle(s) were observed in 25 slides from the slides of the 50 blocks reviewed. Very large amounts of these particles accumulated in macrophages in the lymph nodes and omentum, but significant amounts were also seen in cells in the ovaries and fallopian tubes. **Figure 2** illustrates the findings in this case viewed with polarized light.

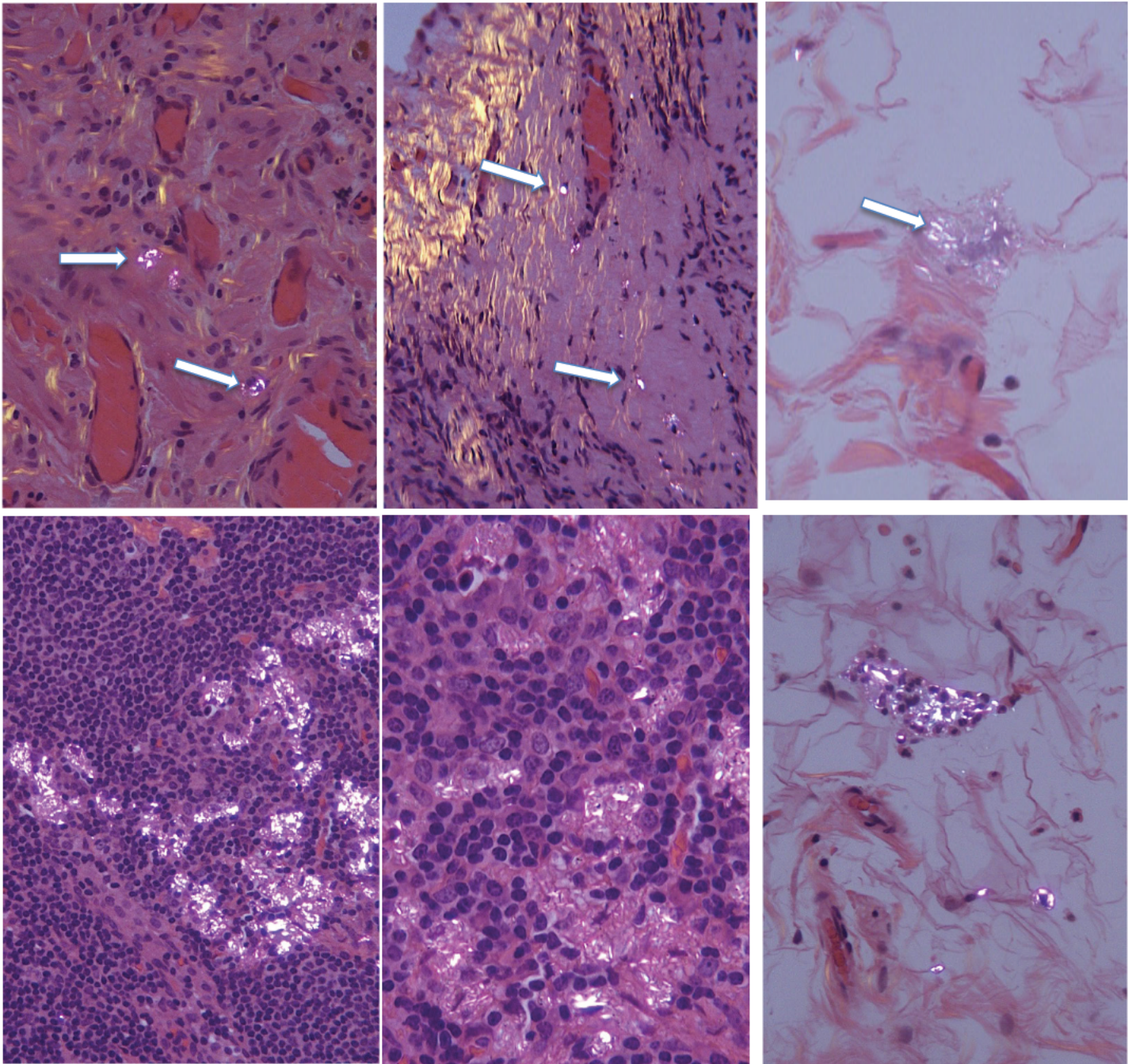


Figure 2. All images with polarized light microscopy. **Top Left.** High-power microscopic view of birefringent particles within cells (arrows) in the wall of the left fallopian tube. Original magnification 400X. **Top Center.** High power microscopic view of individual birefringent particles (arrows) within a fibrotic area of the right fallopian tube. Original magnification 400X. **Top Right.** High-power view of a cluster of birefringent particles (arrow) in a focus of chronic inflammation in the fat and soft tissue of the left gutter. Original magnification 400x. **Bottom Left.** Low power microscopic view of large numbers of birefringent particles in macrophages within a right external iliac lymph node. Original magnification 200X. **Bottom Center.** High power view of right iliac node showing many birefringent particles and fibers. Original magnification 400X. **Bottom Right.** Cluster of birefringent particles and fibers in a section of omentum. Also, scattered individual particles. Original magnification 400X. All images stained with Hematoxylin and Eosin.

Our past experience and the medical literature on the diagnosis of talc in tissues (see references) indicate that the number of birefringent particles in histological sections is robustly correlated with the number of talc particles found by SEM/EDS, since talc is a strongly birefringent material. Also, talc is more likely to be subsequently found by SEM/EDS in tissue sections where 1) the number of birefringent particles by polarized light microscopy is greatest, and 2) the anatomic location of the tissues is most consistent with the expected migration or dissemination patterns for the talc, given its initial application/exposure site (references 1-2).

Taking these factors into consideration, five paraffin tissue blocks from Ms. Gallardo's [REDACTED] surgery (A8, B18, I2, L2, O2), respectively representing [REDACTED] (A8), [REDACTED] (B18), [REDACTED] (I2), [REDACTED] (L2), and [REDACTED] (O2) were selected for further studies. All five of these paraffin tissue blocks were studied by the *in situ* scanning electron microscopy technique using variable pressure as described by Thakral and Abraham (2007, reference 7), in which the paraffin block may be studied directly in the scanning microscope chamber. The blocks were handled with our standard protocol to prevent contamination of the blocks in our laboratory. This protocol begins with the handling of the blocks using powder-free gloves on pre-cleaned surfaces. The blocks were then sectioned, removing ~50 micrometers of tissue and paraffin using a rotary microtome with a new, stainless steel blade. This sectioning was done to remove any surface contamination from previous storage and handling. After the fresh surface is exposed, the blocks were placed in a pre-cleaned covered container to prevent air particulate contamination, and then transferred to the Electron Microscopy Laboratory. There, blocks were again handled with particle-free gloves on pre-cleaned surfaces, and the blocks were washed in distilled deionized water for ≥ 2 minutes to remove soluble surface materials such as sodium chloride and sodium phosphate used in processing for histology. When not being examined in the SEM chamber, the blocks were always maintained in closed plastic stub container boxes to provide secure storage and to obviate lab contamination. An example of a paraffin block studied in this case is shown in **Figure 3**.

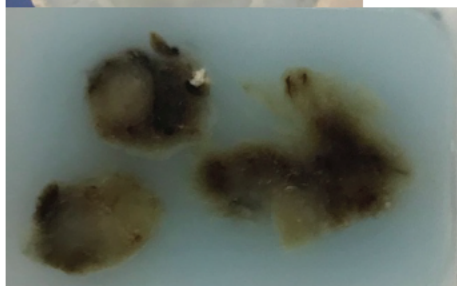


Figure 3. One of the blocks (A8, left tube) examined by SEM/EDS in this case. **Top:** The identification for the block is on the side of the cassette. **Below:** Picture of the cut tissue surface of the block (examined by SEM/EDS).

Tissue surfaces were studied with a Hitachi SU6600 field emission SEM with an Oxford EDS, with Oxford instrument software being Aztec 4.1 SP1. EDS detector model was X-Max 50 SDD. The backscatter mode of the microscope was used to highlight mineral particles within the tissue resulting from atomic number contrast.

Areas of tissue in the sectioned block surfaces were examined with a systematic rastering technique involving sequential fields at relatively low magnification 200-500x, then when particles were seen, higher magnification was used to show morphological characteristics and to do spectral analysis. In this study, images of backscattered or secondary electrons were acquired using 15 kV accelerating voltage, 10 mm working distance, small beam spot, aperture #1, and 60 Pa vacuum (VP-SEM mode). EDS signals were acquired in either the spot analysis or mapping mode, with dead time <20% and signal counts ~3000-5000 cps. Electron beam penetration depth under the conditions used is estimated to be 2.5 micrometers. Image files were named after the number of EDS site ID, which was consecutive from 1. Spectrum ID was also serial coded consecutively from 1. Once the images or spectra are acquired, the assigned serial ID cannot be changed or replaced.

In studying the blocks of Ms. Gallardo by SEM/EDS, a total of 208 talc particles/fibers were found in single ~2-micrometer planes of her tissue

blocks (all listed in **Table 1** on the next page). These particles/fibers were all within 5% of the accepted Mg/Si atomic weight percent ratio of 0.649 for talc and found in all 5 blocks studied. The talc fibers identified all met the accepted criteria for a fiber of length to width ratio of >3:1 and approximately parallel sides as well as the accepted atomic weight percent ratio of 0.649. Fifteen such fibers were found and identified in **Table 1** with an asterisk (*).

Table 1: Talc block and spectrum numbers and Mg/Si atomic weight % ratios within + 5% of 0.649

Block/ spectrum #	Mg/Si ratio	Block/ spectrum #	Mg/Si ratio	Block/ spectrum #	Mg/Si ratio	Block/ spectrum #	Mg/Si ratio	Block/ spectrum #	Mg/Si ratio
A-8 386	0.645	I-2 142	0.624	L-2 270	0.619	L-2 371	0.638	O-2 577*	0.633
B-18 678	0.645	I-2 146	0.627	L-2 271	0.635	L-2 372*	0.635	O-2 579	0.619
I-2 18	0.621	I-2 147	0.619	L-2 275	0.637	L-2 373	0.641	O-2 580	0.663
I-2 23	0.631	I-2 149	0.636	L-2 277	0.622	L-2 376	0.637	O-2 582	0.634
I-2 38	0.631	I-2 150	0.629	L-2 278	0.648	L-2 377	0.642	O-2 584	0.676
I-2 58	0.638	I-2 151	0.619	L-2 279	0.638	L-2 378	0.619	O-2 585	0.628
I-2 59	0.628	I-2 155	0.642	L-2 280	0.638	L-2 379	0.657	O-2 586	0.629
I-2 61	0.621	I-2 156	0.635	L-2 281	0.647	L-2 380	0.621	O-2 588	0.648
I-2 68	0.631	I-2 162	0.619	L-2 282	0.622	L-2 381	0.632	O-2 590	0.665
I-2 72	0.672	I-2 163	0.622	L-2 283	0.642			O-2 593	0.678
I-2 73	0.627	I-2 164	0.625	L-2 284	0.640	O-2 471	0.645	O-2 595	0.625
I-2 74	0.641	I-2 165	0.640	L-2 285	0.645	O-2 473	0.651	O-2 596	0.633
I-2 77	0.645	I-2 176	0.621	L-2 286	0.648	O-2 516	0.667	O-2 599	0.654
I-2 82	0.620	I-2 177	0.639	L-2 287	0.655	O-2 517	0.652	O-2 606	0.654
I-2 83	0.655	I-2 178	0.651	L-2 288	0.632	O-2 518*	0.657	O-2 608*	0.638
I-2 88	0.618	I-2 180	0.635	L-2 289*	0.640	O-2 519	0.618	O-2 609	0.626
I-2 89	0.679	I-2 183	0.622	L-2 291	0.632	O-2 521	0.641	O-2 611	0.621
I-2 92	0.639	I-2 185	0.634	L-2 296	0.624	O-2 522	0.651	O-2 612	0.623
I-2 95	0.665	I-2 187	0.650	L-2 300	0.619	O-2 530	0.627	O-2 613	0.623
I-2 103	0.654			L-2 302	0.654	O-2 533	0.652	O-2 614	0.644
I-2 104	0.656	L-2 210	0.654	L-2 309	0.626	O-2 535	0.642	O-2 616	0.663
I-2 106	0.656	L-2 215	0.628	L-2 311	0.638	O-2 536	0.631	O-2 618	0.636
I-2 113	0.671	L-2 220	0.635	L-2 312	0.640	O-2 537	0.674	O-2 620	0.657
I-2 118	0.646	L-2 223*	0.641	L-2 314	0.635	O-2 538*	0.657	O-2 623	0.652
I-2 119	0.637	L-2 224	0.664	L-2 320	0.618	O-2 539*	0.626	O-2 624	0.655
I-2 120	0.636	L-2 225	0.639	L-2 328	0.630	O-2 540	0.625	O-2 625	0.681
I-2 122	0.621	L-2 228	0.630	L-2 330	0.627	O-2 542	0.621	O-2 626	0.667
I-2 123	0.628	L-2 234*	0.640	L-2 331	0.638	O-2 543	0.666	O-2 627	0.647
I-2 124*	0.621	L-2 237	0.649	L-2 332	0.645	O-2 545	0.625	O-2-630	0.638
I-2 125	0.620	L-2 240	0.628	L-2 333*	0.617	O-2 546	0.622	O-2-633	0.634
I-2 126	0.622	L-2 242	0.633	L-2 337	0.632	O-2 547	0.630	O-2-638*	0.641
I-2 127	0.629	L-2 243	0.620	L-2 339	0.633	O-2 551	0.633	O-2-639	0.646
I-2 128	0.626	L-2 246	0.636	L-2 341	0.650	O-2 554	0.641	O-2-641	0.619
I-2 130	0.630	L-2 248	0.619	L-2 348	0.628	O-2 555	0.658	O-2-643	0.640
I-2 131	0.625	L-2 252	0.623	L-2 353	0.618	O-2 556	0.639	O-2-644	0.651
I-2 133	0.642	L-2 253	0.633	L-2 354	0.624	O-2 567	0.622	O-2-645	0.653
I-2 134	0.628	L-2 256	0.634	L-2 359	0.660	O-2 571	0.634	O-2-646	0.645
I-2 136	0.634	L-2 257	0.640	L-2 361	0.647	O-2 573	0.656	O-2-648	0.631
I-2 137	0.630	L-2 258	0.618	L-2 362*	0.678	O-2 574	0.642	O-2-649	0.623
I-2 139	0.679	L-2 266*	0.626	L-2 367	0.624	O-2 575	0.618	O-2-650	0.630
I-2 141*	0.637	L-2 268	0.632	L-2 368	0.642	O-2 576	0.628	O-2-651	0.623
O-2-661	0.634	O-2-657	0.659	O-2-656	0.622	O-2-655	0.633	O-2-652	0.630

* Fiber

In the study of the blocks on this case, a total of 795 particles were found and analyzed. Tissues may have carbonaceous material detected in backscattered electron imaging mode by their surface irregularity or other characteristics. Also, in many instances iron, sodium, phosphorus, and calcium may be found in tissues, especially in patients with malignancy. These elements are all considered endogenous to the tissues in this type of study. In the tissues studied of Ms. Gallardo, 298 particles had either a calcium composition, salt, or other combinations of various endogenous elements. Four-hundred-ninety-seven (497) particles had a variety of

constituents indicative of exogenous materials including 208 talc particles/fibers, 157 magnesium silicates outside the 5% criteria for talc, 81 magnesium silicates with other cations and/or anions, 30 fragments/fiber within 5% of the accepted Mg/Si atomic weight percent ratio for tremolite asbestos, a known component of cosmetic talc, and 21 other exogenous particles which included various combinations of metals and/or silicon and/or non-metallic elements. The 30 tremolite fragments/fiber are listed in **Table 2**, below, with block, spectrum number and atomic weight percent ratio for tremolite within 5% of 0.541, the accepted Mg/Si atomic weight percent ratio for tremolite.

Table 2: Tremolite block and spectrum numbers and Mg/Si atomic weight % ratios within $\pm 5\%$ of 0.541

Block/ spectrum #	Mg/Si ratio	Block/ spectrum #	Mg/Si ratio	Block/ spectrum #	Mg/Si ratio	Block/ spectrum #	Mg/Si ratio	Block/ spectrum #	Mg/Si ratio
I-2 5	0.543	I-2 34	0.558	I-2 179	0.562	L-2 249	0.562	L-2 360	0.566
I-2 11	0.552	I-2 47	0.551	I-2 189	0.553	L-2 303	0.565	O-2 581	0.563
I-2 19	0.558	I-2 76	0.562	L-2 222	0.567	L-2 318	0.552	O-2 587	0.567
I-2 27	0.553	I-2 100	0.536	L-2 226	0.557	L-2 345	0.555	O-2 601	0.561
I-2 29	0.551	I-2 108	0.556	L-2 227	0.557	L-2 347	0.555	O-2 653	0.557
I-2 30	0.558	I-2 165	0.554	L-2 233	0.536	L-2 352	0.562	O-2 654*	0.537

* Fiber

The technique used in the study of Ms. Gallardo's tissues examines an extremely small volume of tissue. Comparable studies have been done with asbestos fibers in tissue sections (reference 7), and the finding of one fiber in a tissue section comparable to the amount of tissue studied here would indicate at least 100 fibers per gram of tissue which is indicative of a substantial exposure. If similar approaches were applied to the findings of this study, indications are that enormous amounts of talc were present in the patient's pelvic tissues. The findings of 208 talc particles/fibers spread across 5 out of 5 paraffin tissue blocks by analytical microscopy, using this approach, indicates that a very significant amount of talc is present within the tissues. In published studies (references 1, 2, 5, 9), significant numbers of talc particles were detected in pelvic tissues in women with ovarian cancer and a history of perineal talc use. The finding of 15 talc fibers is particularly significant in that the IARC lists talc fibers as a Group 1 carcinogen (Reference 10). The finding of one fiber with the magnesium/silicon atomic weight percent ratio of a tremolite asbestos fiber, a known and widely accepted carcinogen and a known component of cosmetic talc found in the pelvic tissues (References 11-13) is similarly of great importance in linking Ms. Gallardo's ovarian cancer to cosmetic talc exposure.

Ms. Gallardo has 78 talc particles/fibers in a single plane of one paraffin block of tissue of the omentum by SEM/EDS. Four of five hematoxylin and eosin stained slides of omentum had birefringent particles/fibers on polarized light examination. She has no history of previous abdominal surgery. The numbers of birefringent particles in cells and tissues by polarized light examination indicates both very extensive exposure and retention of minerals in her body. Published studies show that exogenous particles enter the female genital tract and may migrate to multiple sites in the pelvis (references 2, 14-16). It is also well-known that the omentum is a common site of metastasis of ovarian carcinoma. Given the extensive burden of particles/fibers in the lymph nodes of this case, migration to the omentum directly or via lymphatics similar to the migration of metastatic tumor cells would be expected.

Figure 4 on the following page shows the morphology and spectra of two examples of talc detected in Ms. Gallardo, one non-fibrous and the other fibrous (block L-2, spectrum 237; block L-2, spectrum 234 respectively). In both these instances, the atomic weight % ratio of magnesium to silicon is the ratio expected for talc (spectrum 237 = 0.649, spectrum 234 = 0.640, the first exactly at the accepted ratio of 0.649 and the other within $\pm 5\%$ of the accepted ratio). In the image field showing the morphology of the particle of spectrum 237, six other particles are visible labeled 238-243. Of these, 240, 242, and 243 are talc and 238, 239, and 241 are magnesium silicates outside the 5% criteria for talc. Within the image field showing the morphology of the fiber of spectrum 234, two other particles (235 and 236) are visible and these are external mineral particles. The magnesium, silicon, and oxygen peaks are labeled by the software of the instrument, which is periodically checked to assure that known elemental materials are properly identified.

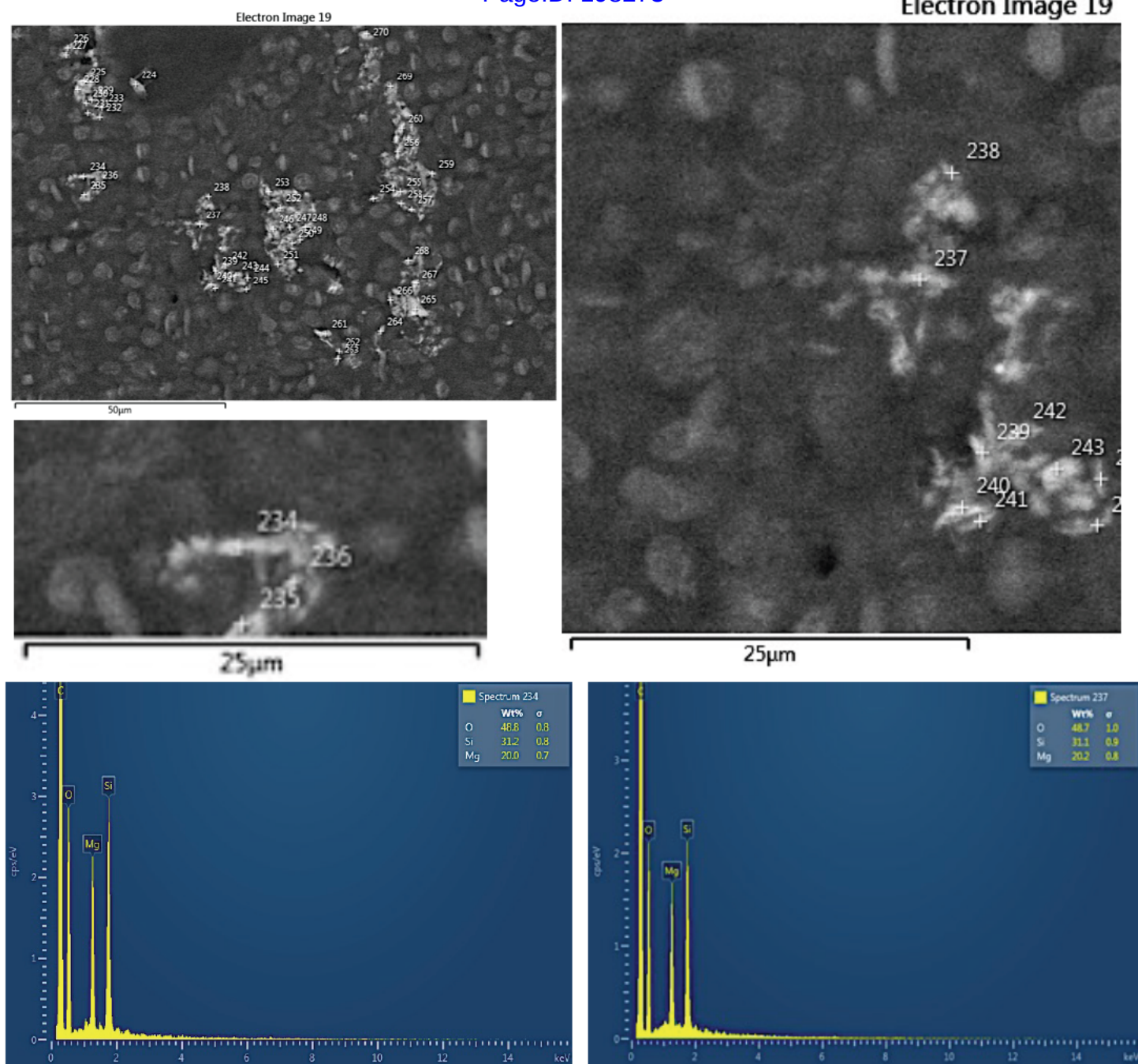


Figure 4. Upper Left. Low magnification SEM image (19) of particles in an area of a lymph node in a paraffin tissue block of the left external iliac lymph nodes (L-2) in backscatter mode. Numerous particles and fibers within cells and tissue are visible. **Upper Right.** An area near the center of the low magnification image is shown at higher magnification so that individual particles can be seen as well as their labels. Particles in this field have varying shapes and are all less than 5 microns in greatest dimension. The particle labeled 237, whose spectrum is shown below, is a talc particle visible in the center left of the image. Of the other particles, 240, 242, and 243 are all talc particles by EDS within 5% of the accepted Mg/Si ratio of 0.649. **Lower Right** EDS spectrum of particle 237 with magnesium, silicon, and oxygen labeled. Magnesium and silicon have the atomic weight % ratio expected for talc, 0.649 which is at the accepted ratio of 0.649. **Middle Left.** Higher magnification of the SEM image (19) of a fiber and surrounding particles in the middle left area of the low magnification image. This fiber is labeled 234, is within tissue, and using the scale on the photo has a length to width ratio of $> 5:1$. **Lower Left** The EDS spectrum of fiber 234 is shown with magnesium, silicon, and oxygen labeled. Magnesium and silicon have the atomic weight % ratio expected for talc, 0.640 which is within $\pm 5\%$ of the ratio 0.649.

Figure 5 below shows the fiber with the Mg/Si atomic weight percent ratio within 5% of tremolite (0.541) found in the tissue of the omentum in block O-2, site 33 electron image 85 and spectrum 654. It has a length to width aspect ratio greater than 5:1. The finding of one fiber plus many fragments with Mg/Si raatios within 5% of tremolite asbestos by the method used here is highly significant since this form of asbestos is a known component of cosmetic talc and has been shown in recent tissue digestion studies of pelvic tissues to be found in women using talc for personal hygiene. (Reference 11 Steffen et al 2020).

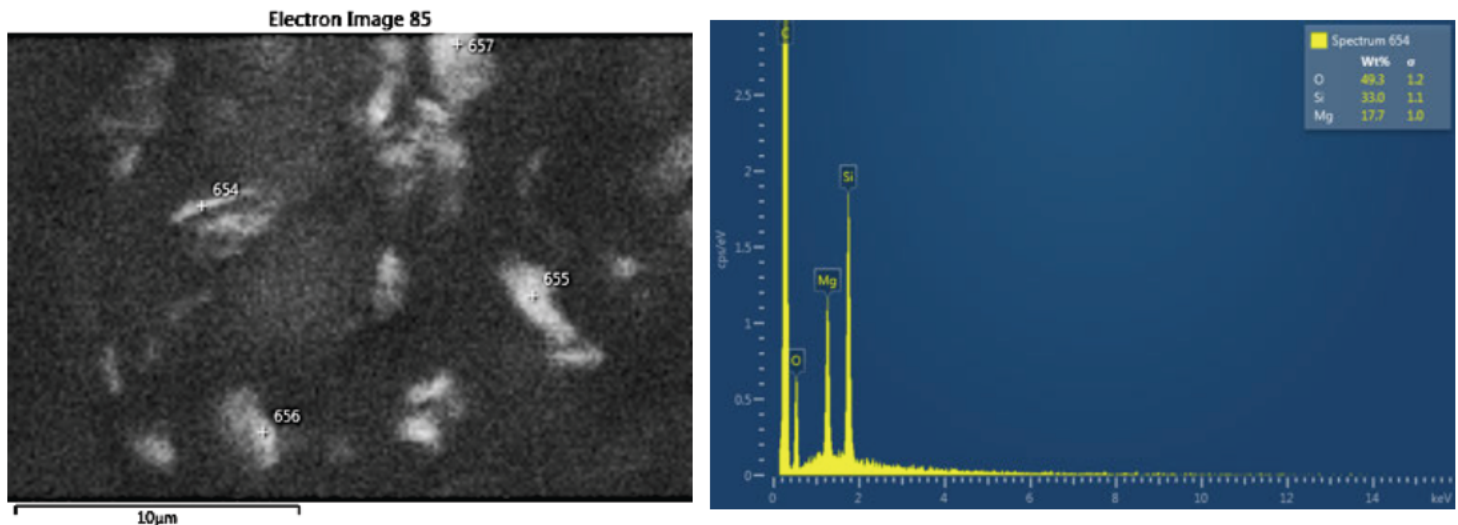


Figure 5. Left SEM image (85) of small particles and a definite fiber labeled 654 in the upper in left portion of this image of omental tissue (block O-2) with spectrum numbers. The fiber has parallel sides and an aspect ratio >5:1. **Right** Spectrum of fiber 654 showing Mg/Si atomic weight percent ratio of 0.536 which is within 5% of the accepted tremolite Mg/Si ratio of 0.541.

Therefore, based on the findings of this case, it can be stated to a reasonable degree of medical certainty, that the talc and tremolite particles/fibers found in the tissues of Ms Gallardo are contributory evidence for a causal link between the presence of these materials and the development of her ovarian cancer. All opinions expressed in this report are to a reasonable degree of medical and scientific certainty.

Sincerely,

John J. Godleski, MD

John J. Godleski, MD
Professor Emeritus of Pathology

References:

1. McDonald, SA, Fan Y, Welch, WR, Cramer, DW, Stearns, RC, Sheedy, L, Katler, M, Godleski JJ. Correlative polarizing light and scanning electron microscopy for the assessment of talc in pelvic lymph nodes. *Ultrastruct Pathol* 43:13-27. 2019. DOI 10.1080/01913123.2019.1593271. PMID: 30898001.
2. McDonald SA, Fan Y, Welch WR, Cramer DW, Godleski JJ. Migration of talc from the perineum to multiple pelvic organ sites: five case studies with correlative light and scanning electron microscopy. *Am J Clin Pathol* 152: 590-607, 2019. <https://doi.org/10.1093/ajcp/aqz080>. PMID: 31305893 PMCID: PMC6779257.

3. McDonald SA, Fan Y, Rogers RA, Godleski JJ. Magnesium/silicon atomic weight percent ratio standards for the tissue identification of talc by scanning electron microscopy and energy dispersive X-ray analysis. *Ultrastruct Pathol* 43: 248-260, 2019. DOI 10.1080/01913123.2019.1692119. PMID: 31736386.
4. Campion A, Smith KJ, Fedulov AV, Gregory DZ, Fan Y, **Godleski JJ**. Identification of Foreign Particles in Human Tissues Using Raman Microscopy *Analytical Chemistry* **2018** 90 (14), 8362-8369 DOI: 10.1021/acs.analchem.8b00271 PMID:29894163
5. Sato E, McDonald SA, Fan Y, Peterson S, Brain JD, Godleski JJ: Analysis of particles from hamster lungs following pulmonary talc exposures: implications for pathogenicity. *Part Fibre Toxicol* 2020; 17:20. <https://doi.org/10.1186/s12989-020-00356-0>. PMID: 32498698 PMCID: PMC7271432.
6. Johnson KE, Popratiloff A, Fan Y, McDonald S, Godleski JJ. Analytic comparison of talc in commercially available baby powder and in pelvic tissues resected from ovarian carcinoma patients. *Gynecol Oncol* 2020; 159: 527-533. PMID: 32977988.
7. Thakral C and Abraham JL. Automated scanning electron microscopy and X-ray microanalysis for in situ quantification of gadolinium deposits in skin. *Microscopy* 2007; 56: 181-187. PMID: 17951398.
8. Roggli VL, Pratt PC. Numbers of asbestos bodies on iron-stained tissue sections in relation to asbestos body counts in lung tissue digests. *Hum Pathol* 1983; 14: 355-361. PMID: 6299925.
9. Cramer DW, Welch WR, Berkowitz RS, Godleski JJ. Presence of talc in pelvic lymph nodes of a woman with ovarian cancer and long-term genital exposure to cosmetic talc. *Obstet Gynecol* 2007; 110: 498-501. PMID: 17666642
10. International Agency for Research on Cancer. [Agents classified by the IARC monographs, volumes 1–129](http://monographs.iarc.fr/ENG/Classification/index.php). [homepage on the internet] Lyon: IARC; [cited 2021 May 19; updated 2021 Mar 26]. Available from: <http://monographs.iarc.fr/ENG/Classification/index.php>.
11. Steffen JE, Tran T, Yimam M, Clancy KM, Bird TB, Rigler M, Longo W, Egilman DS. Serous Ovarian Cancer Caused by Exposure to Asbestos and Fibrous Talc in Cosmetic Talc Powders-A Case Series. *J Occup Environ Med*. 2020 Feb;62(2):e65-e77. doi: 10.1097/JOM.0000000000001800. PMID: 31868762.
12. Gordon R, Fitzgerald S, Millette J. Asbestos in commercial cosmetic talcum powder as a cause of mesothelioma in women. *Int J Occup Environ Health*. 2015;21(4):347-8. doi: 10.1080/10773525.2015.1122368.
13. Health effects of tremolite. This official statement of the American Thoracic Society was adopted by the ATS Board of Directors, June 1990. *Am Rev Respir Dis*. 1990 Dec;142(6 Pt 1):1453-8. doi: 10.1164/ajrccm/142.6_Pt_1.1453. PMID: 2252267.
14. Vanneuville G, Mestas D, Le Bouedec G, Veyre A, Dauplat J, Escande G, Guillot M. The lymphatic drainage of the human ovary in vivo investigated by isotopic lymphography before and after the menopause. *Surg Radiol Anat*. 1991;13(3):221-6. doi: 10.1007/BF01627990. PMID: 1754957.
15. Shimada C, Todo Y, Yamazaki H, Takeshita S, Okamoto K, Minobe S, Yamashiro K, Kato H. A feasibility study of sentinel lymph node mapping by cervical injection of a tracer in Japanese women with early stage endometrial cancer. *Taiwan J Obstet Gynecol*. 2018 Aug;57(4):541-545. doi: 10.1016/j.tjog.2018.06.012. PMID: 30122575.
16. Geppert B, Lönnerfors C, Bollino M, Arechvo A, Persson J. A study on uterine lymphatic anatomy for standardization of pelvic sentinel lymph node detection in endometrial cancer. *Gynecol Oncol*. 2017 May;145(2):256-261. doi: 10.1016/j.ygyno.2017.02.018. Epub 2017 Feb 10. PMID: 28196672.